Ground-state potential of the Ca dimer from Fourier-transform spectroscopy

O. Allard, A. Pashov,* H. Knöckel, and E. Tiemann
Institut für Quantenoptik, Universität Hannover, Welfengarten 1, 30167 Hannover, Germany
(Received 20 March 2002; published 10 October 2002)

The $B\,^1\Sigma_u^+ \rightarrow X\,^1\Sigma_g^+$ system in $^{40}Ca_2$ was studied by Fourier-transform spectroscopy. Transitions to 730 ground-state levels were induced by the blue-green lines of an Ar^+ radiation and the single-mode radiation of a frequency-doubled continuous-wave Nd:YAG yttrium aluminum garnet laser. An accurate potential-energy curve, which covers 99.8% of the well depth, was derived directly from the experimentally observed differences between ground-state levels. Long-range analysis led to a revised value of the ground-state dissociation energy, 1102.08(9) cm^{-1}, which differs by more than 7 cm^{-1} from the previous experimental determination [C. R. Vidal, J. Chem. Phys. **72**, 1864 (1980)]. A first estimate of the *s*-wave scattering length is reported.

DOI: 10.1103/PhysRevA.66.042503 PACS number(s): 31.50.Bc, 33.20.Kf, 33.20.Vq, 33.50.Dq

I. INTRODUCTION

Alkaline-earth metals currently attract both experimental and theoretical research in the field of cold atom interactions. Cooling and trapping of several species (Mg,Ca,Sr) was motivated by the use of group-II atoms for realization of optical frequency standards (Mg [1,2], Ca [3]) and by the perspective for achievement of quantum degeneracy (Sr [5]). Presently cooling techniques are developed for Ca [6,7] and Sr [8] with which microkelvin and even nanokelvin temperatures were reported.

From the theoretical point of view, the $^1S_0$ ground state and the lack of hyperfine structure for the most abundant isotopes highly reduce the number of collision channels compared with the alkali metals. This significantly simplifies the theoretical description of cold collisions, also in presence of laser fields [9].

An important problem for making reliable theoretical predictions on cold collision phenomena in this area is to obtain accurate interaction potentials for alkaline-earth dimers, including the long internuclear distances. Contrary to the alkali metals, the available spectroscopic information is by no means complete and often with insufficient accuracy. On the other hand, there are several theoretical papers devoted to the long-range dispersion coefficients [10–13], but only for Ba_2, Mg_2, and Sr_2 there is an advanced theoretical picture of their electronic structure [14–16].

In this paper we report on an accurate determination of the Ca_2 ground-state potential-energy curve (PEC). Our study was motivated by the rapid progress in the development of the Ca frequency standard [4] as well as the recent photoassociation spectroscopy data on the $^1S_0+^1P_1$ asymptote [17].

The $X\,^1\Sigma_g^+$ state has been the subject of several investigations since the early experimental study of the $B\,^1\Sigma_u^+ \rightarrow X\,^1\Sigma_g^+$ so-called green system by Balfour and Whitlock in 1975 [18], where vibrational levels up to $v''=7$ were observed. In 1980, Vidal extended the spectroscopic data on the X state using the laser induced fluorescence (LIF) technique [19] and derived new sets of Dunham coefficients for the X and B states describing a total of 5846 observed lines covering vibrational levels from $v''=0$ to 34 with a stated standard deviation $\sigma=0.047$ cm^{-1}. A potential-energy curve for the ground state based on the inverted perturbation approach (IPA) was determined, which allowed the extrapolation of the ground-state dissociation energy from experimental data, 1095.0 ± 0.5 cm^{-1}. The calculated eigenenergies of this IPA potential, however, do not agree with the term energies calculated with the Dunham coefficients within the 0.03-cm^{-1} uncertainty stated in Ref. [19]. Moreover, we found systematic deviations for high v'' or high J'' quantum numbers, which reached 3.4 cm^{-1} for the level with $v''=21$ and $J''=102$.

Unfortunately, we could not check the accuracy of either the existing PEC or the Dunham coefficients directly by comparing with the primary experimental data, since they were lost [20]. Therefore, we decided to undertake a spectroscopic study in order to collect new data needed for the accurate description of the ground-state PEC and especially near the dissociation limit.

After a brief description of the experimental arrangement in Sec. II, we present the field of spectroscopic data obtained for the ground state (Sec. III). In Sec. IV we construct the ground-state potential-energy curve and discuss the reliability of its long-range part. Here also an improved set of Dunham coefficients for the B state is given.

II. EXPERIMENT

Calcium dimers were formed in a stainless steel heat pipe oven with a length of 960 mm, a diameter of 34 mm, and a wall thickness of 2 mm. The oven was filled with ≈ 5 g of Ca (natural isotopic composition, 96.94% of ^{40}Ca) and He as buffer gas with pressure up to 60 mbars and heated up to 1350 K. After accumulating approximately 100 h of operation during several runs in air under these conditions, just a very thin layer of corrosion was present on the outer surface of the tube. But the time of a single run was limited mainly by the formation of solid calcium closing the optical path in about 5 h. This working time was sufficient to ensure correct recordings.

*On leave from the Institute for Scientific Research in Telecommunications, ul. Hajdushka poliana 8, 1612 Sofia, Bulgaria.

TABLE I. Transitions of the B-X and an unassigned system in $^{40}Ca_2$ excited with a single-mode frequency-doubled cw Nd:YAG tunable laser.

v'	J'		v''	J''	$\nu[\mathrm{cm}^{-1}]$
0	97	$\leftrightarrow$	7	96	18787.6738(56)
0	101	$\leftrightarrow$	7	102	18788.3028(60)
1	111	$\leftrightarrow$	13	110	18787.3804(66)
2	21	$\leftrightarrow$	9	20	18788.3639(60)
2	25	$\leftrightarrow$	9	26	18788.2842(61)
2	69	$\leftrightarrow$	11	70	18787.6237(68)
2	77	$\leftrightarrow$	12	76	18788.3853(60)
2	99	$\leftrightarrow$	15	100	18788.3088(61)
3	57	$\leftrightarrow$	14	56	18788.3059(62)
3	85	$\leftrightarrow$	18	84	18788.3471(61)
4	27	$\leftrightarrow$	16	28	18787.4502(105)
4	79	$\leftrightarrow$	24	80	18787.5046(73)
	11	$\leftrightarrow$	24	12	18787.4862(78)
	33	$\leftrightarrow$	15	32	18788.4259(68)
	45	$\leftrightarrow$	22	44	18787.5811(73)
	55	$\leftrightarrow$	16	54	18787.4308(65)
	59	$\leftrightarrow$	16	60	18787.3778(64)

The sample was irradiated using the 514-nm, 496-nm and 476-nm lines of a multimode argon ion laser (Coherent CR-2000K, used output power of 1–1.5 W), which are known to excite a number of transitions in the $^{40}Ca_2$ B-X system listed in Ref. [19]. In our experiment most of these transitions were observed and we were also able to determine the ground-state level of the previously unassigned transition at 514.5 nm to the B state $v'=9$, $J'=83$ level as $v''=24$, $J''=84$.

Comparing the Franck-Condon factors for the B-X system, we found that the most favorable conditions for inducing transitions to the ground-state levels near the dissociation limit are realized when exciting the B state level with $v'=2$. From the available laser sources we chose a single-mode frequency doubled cw Nd:YAG laser (yttrium aluminum garnet) (532.4 nm), since two convenient transitions fall into its tuning range ($\sim$90 GHz), namely, (2,21)$\leftarrow$(9,20) and (2,25)$\leftarrow$(9,26). The laser linewidth was less than 10 kHz and the output power was typically 150 mW. An untunable high power cw green Nd:YAG laser (Coherent V-10, applied output power 1–3 W) was also used because of the accidental coincidence of its frequency (within the Doppler profile) with the frequency of the (2,21)$\leftarrow$(9,20) transition. Transitions excited by both Nd:YAG lasers in the range of 18787.2–18788.7 cm^{-1} are listed in Table I. For several of them it is not possible to assign an upper state level from the B state. Probable assignments could be to the $A\,^1\Sigma_u^+$ state or to the recently reported $^1\Pi_u$ state, observed in the study of Ca dimers deposited on argon and neon van der Waals clusters [21]. In the spectral region of interest, however, few or no data are available for these states and the problem of assignment was postponed. Nevertheless the ground-state assignment could be obtained unambiguously.

Laser induced fluorescence was collected in a direction antiparallel to the laser beam propagation and was recorded by a photomultiplier tube (Hamamatsu, R928) through a Bruker IFS 120HR Fourier-transform spectrometer with absolute accuracy better than 0.01 cm^{-1} (relative accuracy better than 0.001 cm^{-1}) at 500 nm. Each collected spectrum of the $B\rightarrow X$ system results typically from 20 scans, while for progressions extending up to the dissociation limit 40 scans were averaged. The instrumental resolution was chosen to be 0.05 cm^{-1}–0.06 cm^{-1}, which is a compromise between the expected value of the observed linewidths and a reasonable time of recording.

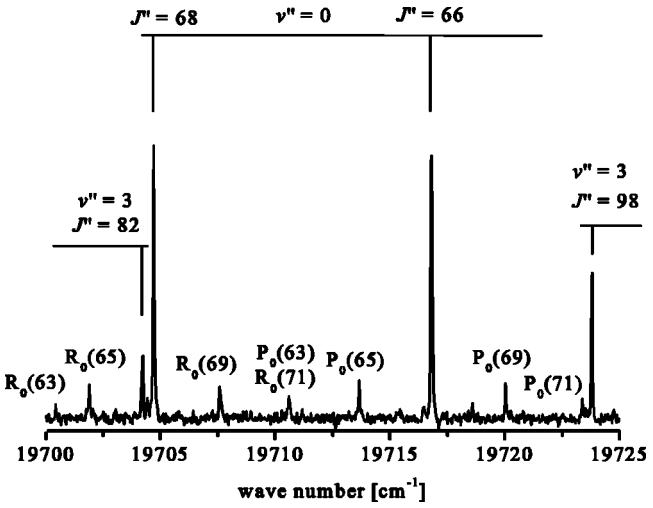

FIG. 1. Example of laser induced fluorescence spectrum of the $B\,^1\Sigma_u^+\rightarrow X\,^1\Sigma_g^+$ system in $^{40}Ca_2$, excited by the 514.5 line of the Ar^+ laser. Collisional induced lines are denoted with $P_{v''}(J')$ and $R_{v''}(J')$.

Different optical filters were used, especially color glass filters to suppress radiation from the oven, and interference filters ($\Delta\lambda\sim 8$ nm) centered on 550 and 546 nm for the observation of the last lines of the progressions going to the dissociation limit.

III. RESULTS

In Fig. 1 a portion of the $B\,^1\Sigma_u^+\rightarrow X\,^1\Sigma_g^+$ transitions excited with the 514.5-nm line of the Ar^+ laser is shown. The typical width of the observed lines is 0.07 cm^{-1}. Taking into account the Doppler broadening at 1350 K (0.05 cm^{-1}) and the instrumental linewidth (0.04 cm^{-1}), the residual width of $\approx$0.02 cm^{-1} remains most likely due to collisions of Ca_2 molecules with the buffer gas and the atomic Ca. As the collisional broadening was not a purpose of this study, a thorough investigation of the line profiles was not performed. Nevertheless the above-determined residual width gives some impression about the order of magnitude of the collisional linewidths and line shifts, which are expected to be comparable.

The uncertainty in the positions of the line centers was estimated by a simulation, which takes into account the signal-to-noise ratio (SNR), the linewidths, and the number of experimental points falling on a line profile (typically six to eight). In this way, for lines with SNR >5 the uncertainty was estimated to be lower than 0.01 cm^{-1} but reaches

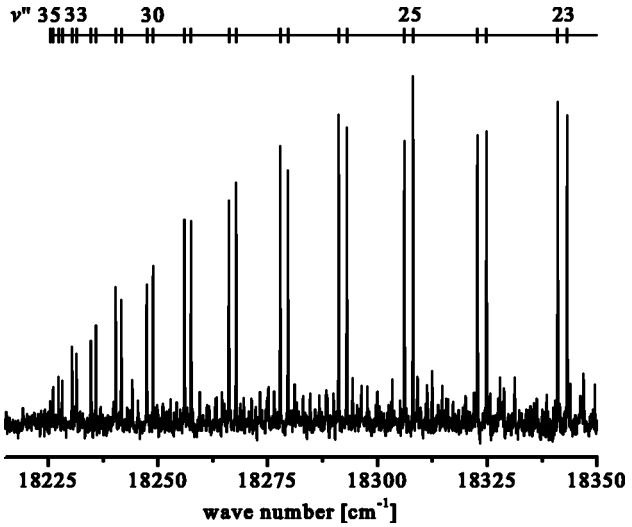

FIG. 2. Vibrational progression from the (2, 21) B state level, excited by a frequency-doubled single-mode cw Nd:YAG laser. The weak lines are due to collisional induced transitions.

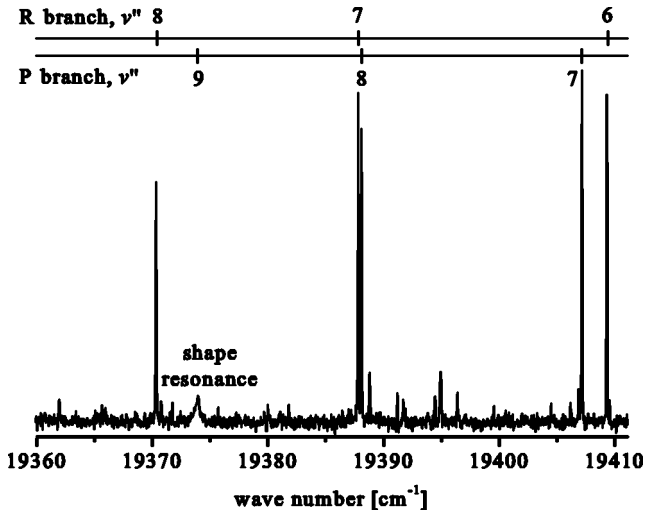

FIG. 3. Example of shape resonance for $v''=9$, $J''=160$ in the vibrational progression from the (2, 161) B state level, excited by the 514.5-nm line of the Ar^+ laser.

0.03 cm^{-1} for SNR$\sim$1–2. In order to improve the accuracy of our measurements, certain LIF spectra were recorded several times.

Spectroscopic information about the energy levels near the dissociation limit was collected by tuning the Nd:YAG laser frequency to the (2,21)$\leftarrow$(9,20) and (2,25)$\leftarrow$(9,26) transitions. A vibrational progression reaching $v''=35$ for $J''=20,22$ is shown in Fig. 2. Collisionally induced satellites are readily followed for v'' up to 31. It should be noted that both the (2,21)$\leftarrow$(9,20) and (2,25)$\leftarrow$(9,26) transitions are excited simultaneously and accompanied by the much stronger (0,101)$\leftarrow$(7,102) transition, because of the overlap of their Doppler profiles (see Table I). Due to the strong fluorescence from $v'=0$, $J'=101$ level to the continuum of the ground state, progressions from the levels (2,21) and (2,25) to the energy region close to the dissociation limit are always recorded on a relatively strong background of bound-free emission, which affects the signal-to-noise ratio.

In Fig. 4 we present the range of the 730 ground-state energy levels involved in the observed B-X transitions. A comparison with the data set from Ref. [19] shows that we covered the same range of J'' quantum numbers ($10\leqslant J''\leqslant 164$), but more levels with high vibrational quantum numbers were collected (four levels with $v''=34$ and two with $v''=35$). The observation of the $v''=35$ itself has already indicated that the asymptotic behavior of the earlier reported ground-state potential needs revision as with the given value of the dissociation energy (1095.0 ± 0.5 cm^{-1} [19]), the last bound level for $J''=20,22$ would have been $v''=34$. We also found that with the sets of Dunham coefficients from Ref. [19] it is not possible to reproduce all the observed B-X transitions within the stated uncertainty (0.047 cm^{-1}). Transitions involving high v'' and high J'' deviate systematically from the predicted frequencies by up to 3.4 cm^{-1}.

In addition to the transitions in Table I, induced by the laser radiation, the experimental information was enriched by several collisionally induced transitions. Figure 1 shows an example of such satellites, corresponding to transitions from the B state levels with $v'=5$, $J'=63,65,69,71$ and populated by collisions from the $v'=5$, $J'=67$ level.

For several rovibrational levels, which in the presence of centrifugal barrier lie above the dissociation limit of the ground state, additional broadening (up to 0.5 cm^{-1}, see Fig. 3) was observed due to significant tunneling probability through the barrier. The linewidths for such shape resonances were not used in the procedure for the determination of the potential-energy curve. Therefore, the agreement between the calculated widths with the experimental ones confirmed the consistency of the determined PEC.

IV. CONSTRUCTION OF PEC

Based on the LIF technique, the current experiment provides relatively little data about the excited states. So it is not reasonable to try to describe the experimentally observed transition frequencies by simultaneously fitting the potential-

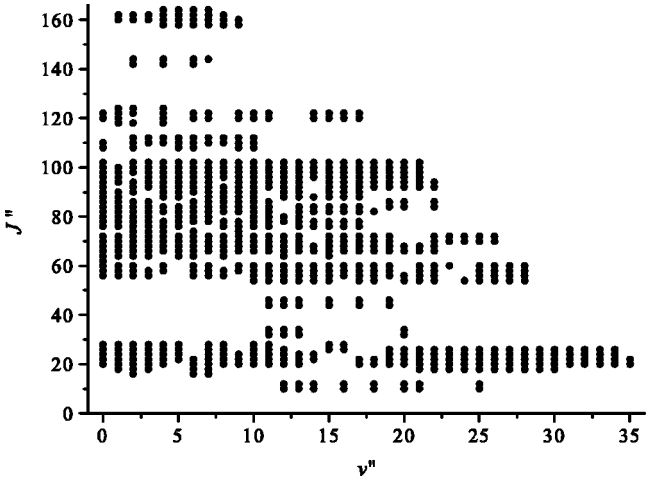

FIG. 4. The range of the v'' and J'' quantum numbers of the observed levels in the $X\,^1\Sigma_g^+$ state of $^{40}Ca_2$.

energy curves of both involved electronic states. Instead the information that concerns only the ground state can be extracted from the spectra. By comparing the frequencies of the transitions, which originate from a common excited-state energy level, one directly determines the differences between the corresponding ground-state levels. The fitting procedure then tries to find such a potential-energy curve, which reproduces these experimentally measured differences.

An advantage of this approach is that the influence of the excited-state level positions is excluded. The excited state is expected to be perturbed [19], and in addition, as we already mentioned in Sec. III, the collisional shifts are comparable with the measurement accuracy. Because in practice the excited-state levels are more sensitive to collisions; by fitting only the differences between the ground-state levels we decrease also the influence of this effect. If fluorescence is induced by a single-mode laser which is not tuned exactly to the center of the absorption profile all the transition frequencies will be Doppler shifted. This shift is frequency dependent and therefore it will not be the same for the different transitions and strictly speaking cannot be completely eliminated when the differences are calculated. In our case this may lead to residual ''shifts'' of the differences, which we estimated as not exceeding 0.003 cm^{-1} and therefore could be neglected within the given experimental uncertainty.

Due to the large number of observed transitions (more than 2800), we restricted the possible combinations of line frequencies within a fluorescence progression only to pairs of one P and one R line. That is, we calculated only differences between each P and all R lines of a given progression. By ignoring the differences among the P lines or the R lines only, the total amount of differences was reduced approximately by a factor of 2.

As it has been already mentioned, some fluorescence progressions were recorded several times. In such cases differences between the ground-state energy levels were determined separately for each record and then statistically averaged with weights calculated from the corresponding line center uncertainties. As a result more than 6500 differences between 730 ground-state levels were obtained (see Fig. 4). The estimated uncertainties of the differences range from 0.004 cm^{-1} to 0.05 cm^{-1} and for 67% of the differences they are below 0.015 cm^{-1}.

For construction of the PEC for the ground-state, two different fully quantum-mechanical methods were used, which are discussed separately in the following sections. Both methods determine the potential curve directly from the experimental observations and the accuracy of a given PEC is evaluated by comparing the differences between its energy levels, found by solving the radial Schrödinger equation, with the experimental differences. Although the representations of the potential for intermediate internuclear distances in both cases are different, the same expression is used for the long-range region:

$$U_{\mathrm{LR}}(R)=D_e-C_6/R^6-C_8/R^8-\cdots. \tag{1}$$

A. Analytic potential

The first method represents the potential as a truncated expansion over analytic functions [22]:

$$U(R)=\sum_{i=0}^{n} a_i\left(\frac{R-R_m}{R+bR_m}\right)^i, \tag{2}$$

where a_i, b, and R_m are parameters (R_m is close to the equilibrium distance). For short and long internuclear distances, the potential is smoothly extended, respectively, for $R\leqslant R_{\mathrm{inn}}$ with

$$A+B/R^{12}, \tag{3}$$

and for $R\geqslant R_{\mathrm{out}}$ with

$$D_e^{\mathrm{X}}-C_6/R^6-C_8/R^8-C_{10}/R^{10}. \tag{4}$$

Initially, it was decided that only a_i had to be determined during the fitting procedure. C_6 and C_8 were fixed to their most recent theoretical values from Refs. [12] and [13], respectively, while A,B,C_{10}, and D_e^{X} were adjusted by the program in order to ensure a smooth connection between the extensions and the analytic form. R_m, b and the connecting points R_{inn} and R_{out} were kept fixed to values, which allow fast convergence of the fitting routine. The fitted parameters were determined in a nonlinear fit (for details see Ref. [22]).

Several analytic potentials were constructed with different numbers of a_i parameters (21, 23, and 39). The inner connecting point R_{inn} was varied between 3.5 Å and 3.7 Å and R_{out}, between 12 Å and 13 Å. The so-defined PECs had similar accuracy and reproduced all the observed differences with a normalized standard deviation $\overline{\sigma}=0.41$ and an absolute standard deviation of 0.0065 cm^{-1}.

B. Numerical potential

The second method defines the PEC as a set of points, whose values are determined by using a modified version of the IPA [23–25]. For connecting the points, cubic spline functions are used. The basic idea of IPA is to iteratively improve an initial potential [usually a Rydberg-Klein-Rees (RKR) one] by adding small corrections. In our case the corrections are also represented in a pointwise form and their parameters are determined by a linear fit procedure, based on the first-order perturbation theory and using the singular value decomposition (SVD) technique (for details see Refs. [25–27]).

For the case of Ca_2 the potential curve was defined initially in the interval 2.7 Å–13.1 Å by using different number of grid points (from 50 to 118). In order to ensure proper boundary conditions for solving the Schrödinger equation the potential was extended by a long-range expansion whose coefficients were determined by fitting the shape of the numerical potential between 12 Å and 13.1 Å with $D_e^{\mathrm{X}}-C_6/R^6-C_8/R^8-C_{10}/R^{10}$. The value of C_6 was fixed close to the theoretical value [12], D_e^{X}, C_8, and C_{10} were fitted, while the connecting point R_{out} was chosen in order to ensure a smooth connection with the pointwise potential.

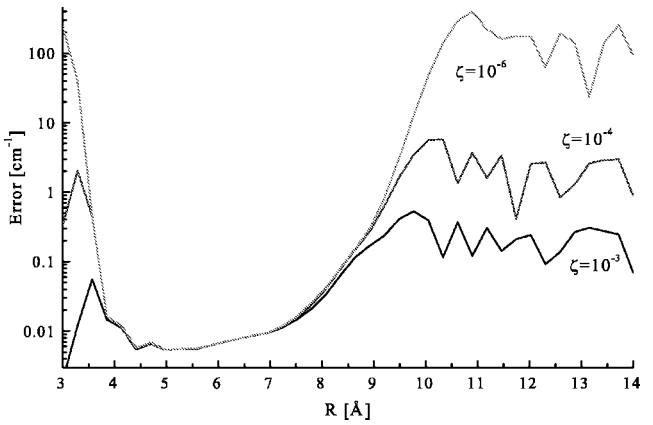

FIG. 5. The standard error (in logarithmic scale) of the points of the numerical potential curve for three different values of the singularity parameter ζ (see the text for details.)

The numerical potentials reproduced the observed differences with a standard deviation of 0.0068 cm^{-1} and $\overline{\sigma} = 0.45$.

By using the SVD technique one is able to determine the fitting parameters, on which the fit depends only weakly [27]. In our case the fitting parameters are the values of the corrections to the potential. Because it is given also in a pointwise form, the set of badly determined parameters may be interpreted as regions of the PEC, which are insufficiently characterized by the given set of experimental data [26]. In Fig. 5 the errors of the fitting parameters for different values of the singularity parameter ζ are presented (for details see Refs. [25,26]). Only parameters whose error does not change with ζ are considered as significant. From Fig. 5 one may conclude that presently the potential for the X state is determined reliably between $\approx$3.5 Å and 9.5 Å. It must be stressed that except for this qualitative treatment, we would avoid the direct interpretation of the errors, presented in Fig. 5 as measurement uncertainties of the derived PEC. This is due to the fact that the fitting procedure restores the shape of the PEC exclusively by searching for an agreement between the calculated energy levels (or differences between levels) and the experimental ones. There is no built-in criterion which can distinguish between the so-called physical and nonphysical shapes. That is why the errors between 9.5 Å and 13 Å should be understood in a purely mathematical sense. By varying the number of fitted parameters and the values of ζ, a variety of PECs (not necessarily with a physical shape) may be obtained, which differ significantly for these internuclear distances. Of course if only smooth and physical curves are considered, this will restrict to some extent the possible variations of the PEC. Such a choice, however, may not be unique, as generally there is no unambiguous criterion for determining which shape is physical and which is not. In contrast, the shape of the potential for 3.5 Å$<R<$9.5 Å is fixed by the available set of experimental data (within the experimental accuracy) and is independent of the number of fitted parameters, as well as of ζ (Fig. 5). We will discuss this problem further in the following section and demonstrate that although the potential accurately reproduces all the experimental data, its shape between 9.5 Å and 13 Å might be constructed in slightly different ways and one should take this into account when using it for extrapolation to larger internuclear distances.

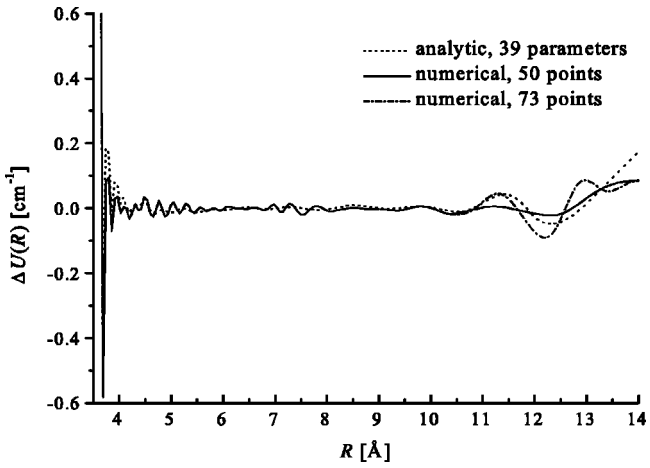

FIG. 6. Differences between two pointwise (50 and 78 points) and two analytic (21 and 39 a_i parameters) presentations of the potential-energy curve for the $X\,^1\Sigma_g^+$ state in $^{40}Ca_2$. The analytic curve defined with 21 parameters is taken as a reference.

C. The $X\,^1\Sigma_g^+$ state dissociation energy

The lack of fine and hyperfine interactions as well as the large energy separation from the excited states make the Ca_2 ground-state a good testing ground to study the possibility of using a spectroscopically determined potential-energy curve for description of cold collisions between two calcium atoms. Therefore, it is of particular interest to investigate how reliable the potential curve is, especially its long-range part and dissociation energy, and whether it is possible to set some reasonable limits on the value of the *s*-wave scattering length.

In the previous sections, ground-state PECs of identical accuracy were derived from the experimentally determined differences between energy levels. The differences between two pointwise (50 and 78 points) and two analytic (21 and 39 a_i parameters) potentials are plotted in Fig. 6. The relatively large deviation for short internuclear distances is explained by the fact that the positions of high-lying energy levels are fairly insensitive to the shape of the steep inner wall of the potential well.

Because all four potentials reproduce the experimental data with similar accuracy, obviously the effect of the fast oscillating differences for intermediate internuclear distances ($<$10 Å) is below the experimental uncertainty. Therefore, these differences could be reduced by improving the accuracy of the experimental data. On the other hand, according to Fig. 5, the potential beyond 9.5 Å is not uniquely determinable. Consequently, the difference in this region may be interpreted as an ambiguity due to the small number of experimental levels close to the asymptote. Indeed, the outer turning points of 712 levels fall in the region of internuclear distances 4.5 Å$<R<$9.5 Å, while there are only 18 in the interval between 9.5 Å and 13.1 Å.

This example demonstrates that the classical turning points of the last observed levels (in our case ~ 13.1 Å) do not always determine the range in which the PEC is accurately known.

An important exception is the case for which the experimental data extend to the long-range region where analytic expression for the shape of the potential is available. If the PEC is already reliably determined beyond the region with small contribution of the exchange energy, the dispersion coefficients could be determined in the fitting procedure.

As an estimation for the exchange energy, we used the expression from Ref. [28]):

$$U_{\mathrm{exch}}(R) = BR^{\alpha}\exp(-\beta R), \tag{5}$$

where the values for the Ca_2 ground-state are $B = 0.067$ a.u., $\alpha = 4.16$ a.u., and $\beta = 1.356$ a.u. At 9.5 Å $U_{\mathrm{exch}}(R)$ is only 0.07 cm^{-1}. This should be compared with the contribution of the weakest dispersive term used, with C_{10}: ~ 1.5 cm^{-1}. Therefore, we examined whether it is possible to describe the experimental data by smoothly extending the PEC after 9.5 Å with the long-range expansion (1) only.

A number of PECs with similar accuracy ($\overline{\sigma} \leqslant 0.45$) was constructed, which had virtually identical shape (both in analytic and numerical representations) for intermediate internuclear separations but different long-range extensions defined by Eq. (1) and including terms with C_6, C_8, and C_{10}. The connecting point was varied between 9.5 Å and 10 Å. Unfortunately, the existing experimental data (18 levels with outer turning points in the range from 9.5 Å to 13.1 Å) are not enough in order to allow reliable determination of contributions due to different dispersive forces. For example, the obtained value of C_6 varied from 0.7×10^7 cm^{-1} $\mathrm{Å}^6$ to 2.01×10^7 cm^{-1} $\mathrm{Å}^6$. Nevertheless the dissociation energy D_e^X was already fairly well constrained between 1101.9 cm^{-1} and 1102.6 cm^{-1}.

A better estimation of D_e^X can be achieved if we restrict the variation of the leading term in the long-range extension C_6 to within 5% of the theoretical prediction of 1.070×10^7 $\mathrm{cm}^{-1}\mathrm{Å}^6$ from Ref. [12]. We prefer this value since the authors give an estimate for its uncertainty: 0.6%. In this way the 5% range used by us seems to be a loose constraint. The remaining parameters, i.e., C_8, C_{10}, and D_e^X and the parameters for the short-range representations were varied within ranges that allowed an accurate description of the experimental data and a smooth connection between the analytic or the pointwise and the long-range sections of the PEC. This narrowed further the possible values for D_e^X between 1101.99 cm^{-1} and 1102.17 cm^{-1}. It is worth mentioning that the lower limit for D_e^X given above is set exclusively by the position of the last observed level ($v''=35, J''=22$). For $D_e^X < 1101.99$ cm^{-1} the calculated differences including this level deviated from the observed ones by more than two times the experimental uncertainty (0.017 cm^{-1}). The interval obtained for C_8 is 1.1×10^8–3.8×10^8 cm^{-1} $\mathrm{Å}^8$, which is in a good agreement with the theoretical value of 3.27×10^8 cm^{-1} $\mathrm{Å}^8$ [13] (see Table II).

TABLE II. Parameters of the long-range expansion for the $X\,^1\Sigma_g^+$ state in $^{40}Ca_2$ applied in this study and compared with the most recent data from the literature.

	This study	Other sources
D_e^X (cm^{-1})	1102.08(9)	1095.0(5) [19]
D_0^X (cm^{-1})	1069.88(9)	
C_6 (cm^{-1} $\mathrm{Å}^6$)	$(1.02$–$1.12)\times 10^7$	$1.070(6)\times 10^7$ [12]
		1.098×10^7 [13]
		1.1510×10^7 [19]
C_8 (cm^{-1} $\mathrm{Å}^8$)	$(1.1$–$3.8)\times 10^8$	3.2710×10^8 [13]
C_{10} (cm^{-1} $\mathrm{Å}^{10}$)	$(3.7$–$17.0)\times 10^9$	4.74×10^9 [13]

If we take $D_e^X = 1102.08 \pm 0.09$ cm^{-1} as a mean estimate for the ground-state dissociation limit, the energy separation between the turning point of the highest observed vibrational level ($v''=35, J''=22$) from the asymptote is only 2.3 cm^{-1}. For comparison, the same separation for the second extensively studied alkaline-earth dimer, Mg_2 ($v''=12$), is 25 cm^{-1}, which was obtained in the recent study devoted to the determination of the magnesium ground-state scattering length [29]. In Table II the parameters of the long-range extension derived in this study are compared with the most recent data from the literature. The value of the dissociation energy for Ca_2 with respect to $v''=0, J''=0$ is $D_0^X = 1069.88(9)$ cm^{-1}.

In Tables III and IV the final parameters of the analytic and the numerical potentials are presented. Their eigenenergies agree with a standard deviation of 0.0035 cm^{-1}. In order to calculate the value of the numerical potential in the range $R < 9.496\,61$ Å, a natural cubic spline [27] through all the grid points should be used. The coefficients for the long range expansion are listed in order to extrapolate beyond $R_{\mathrm{out}} = 9.496\,61$ Å. For short internuclear distances we found that extrapolation of the potential up to $R \approx 3.1$ Å should be sufficient to correctly reproduce the observed energy levels. The factor $\hbar^2/2m$ in the Schrödinger equation [in the system of units: energy, cm^{-1}; length, Å; and mass, atomic mass units (amu)] is expressed as $\alpha^2 m_e 10^{18}/R_\infty (4\pi)^2 m = 16.857\,629\,083/m$ cm^{-1} $\mathrm{Å}^2$ [30]. R_∞ is the Rydberg constant in cm^{-1}, α the fine-structure constant, and m_e the electron mass in amu. For the reduced mass of Ca_2, the value from Ref. [31], $m = 19.981\,295\,578$ amu, is used.

In Fig. 7 we compare the PEC from Table IV (solid line) with the IPA potential from Ref. [19] (squares) near the asymptote. The change of the value of the dissociation energy by more than 7 cm^{-1} compared to Ref. [19] explains the discrepancies between the observed differences and those calculated with the IPA potential by Vidal [19]. Below $v'' = 29$ (classical turning point ~ 8.6 Å) this potential reproduces the experimental data with a standard deviation of 0.1 cm^{-1} (the natural cubic spline was used to interpolate between the points from Ref. [19]). The calculated positions of the levels with higher v'', however, were systematically shifted to lower energies, which leads to disagreements with the experiment reaching 2.7 cm^{-1} for the differences including $v'' = 34$.

TABLE III. Parameters of the analytic representation of the $X\,^1\Sigma_g^+$ state potential-energy curve in $^{40}Ca_2$. The parameters are chosen such that the minimum of the PEC is set to zero.

	$R \leqslant 3.66$ Å
R_{inn}	3.66 Å
A	-0.2977402428×10^3 cm^{-1}
B	0.721345176×10^{10} cm^{-1} Å^{12}
	3.66 Å$< R <$10.00 Å
b	-0.5929
R_m	4.277277 Å
a_0	0.00042747 cm^{-1}
a_1	$-0.25408309276477307\times10$ cm^{-1}
a_2	$0.37961100260114922\times10^4$ cm^{-1}
a_3	$0.38207030202249524\times10^3$ cm^{-1}
a_4	$-0.27439039695467932\times10^4$ cm^{-1}
a_5	$-0.32276334190800926\times10^4$ cm^{-1}
a_6	$0.36311380569301855\times10^3$ cm^{-1}
a_7	$0.63437054218975527\times10^4$ cm^{-1}
a_8	$-0.74015183596084689\times10^4$ cm^{-1}
a_9	$-0.19073891300372907\times10^5$ cm^{-1}
a_{10}	$0.54234739243301759\times10^5$ cm^{-1}
a_{11}	$0.44039230437301106\times10^5$ cm^{-1}
a_{12}	$-0.15538794495452612\times10^6$ cm^{-1}
a_{13}	$-0.83662838135323618\times10^5$ cm^{-1}
a_{14}	$0.21383106708315687\times10^6$ cm^{-1}
a_{15}	$0.15592244922282684\times10^6$ cm^{-1}
a_{16}	$-0.15626087299948314\times10^6$ cm^{-1}
a_{17}	$-0.14671112095921967\times10^6$ cm^{-1}
a_{18}	$0.27754299977223087\times10^5$ cm^{-1}
a_{19}	$0.71290801557933912\times10^5$ cm^{-1}
a_{20}	$-0.12611555040899898\times10^4$ cm^{-1}
	10.00 Å$\leqslant R$
R_{out}	10.00 Å
D_e^X	1102.096077 cm^{-1}
C_6	1.0740×10^7 cm^{-1} Å^6
C_8	2.4505×10^8 cm^{-1} Å^8
C_{10}	1.1691×10^{10} cm^{-1} Å^{10}

D. Molecular constants for the $B^1\Sigma_u^+$ state

The $B\,^1\Sigma_u^+$ state in Ca_2 correlates to the ^1S-^1P atomic asymptote. It is involved as an upper state in the photoassociation process [17] and may be considered as a possible intermediate state for formation of cold calcium molecules. The most recent description of the B state comes from the analysis of the B-X band system in Ref. [19]. In that paper sets of molecular constants for both states were determined by simultaneously fitting them in order to reproduce the observed transition frequencies. As this constants turned out not to be consistent with the experimental observations (see Sec. III), it was necessary to reanalyze the existing information on the B state.

The raw experimental data from Ref. [18] (more than 3800 lines) were not available in electronic form and therefore, in order to reduce our manual work, only 583 transition frequencies of the $B\,^1\Sigma_u^+ \rightarrow X\,^1\Sigma_g^+$ system were chosen, which provide a balanced spread of rovibrational levels in the B state. They resulted in 320 levels spanning the range $0 \leqslant v' \leqslant 16, 21 \leqslant J' \leqslant 161$. Their term energies were calculated by adding the corresponding ground-state level energy (calculated form the newly derived potential from Table IV) to the reported transition frequency. To estimate the uncertainty of the B state energy levels we took into account the reported experimental error of 0.05 cm^{-1} [18], which was reduced in the sense of the statistical average for levels appearing more than once in the selected data set, as well as a ground-state level uncertainty of 0.007 cm^{-1}.

TABLE IV. Parameters of the numerical representation of the $X\,^1\Sigma_g^+$ state potential-energy curve in $^{40}Ca_2$.

R (Å)	U (cm^{-1})	R (Å)	U (cm^{-1})
3.096980	9246.6895	5.678571	636.3741
3.188725	6566.7325	5.809524	684.9589
3.280470	4525.7282	5.940476	728.9235
3.372215	3090.9557	6.071429	768.5976
3.463960	2134.2175	6.202381	804.2551
3.555705	1475.2425	6.333333	836.2419
3.647450	1004.5043	6.464286	864.8746
3.739195	661.4123	6.595238	890.4666
3.830940	410.6117	6.726191	913.2923
3.922685	234.0001	6.857143	933.6417
4.014430	116.0996	6.988095	951.7718
4.106174	44.5437	7.119048	967.8632
4.197920	8.6885	7.250000	982.2159
4.289664	0.1760	7.500000	1005.2497
4.381409	11.9571	7.750000	1023.6698
4.500000	48.5948	8.000000	1038.3262
4.630952	106.9081	8.358974	1054.3861
4.761905	175.7311	8.717949	1066.0579
4.892857	248.8199	9.076923	1074.5969
5.023809	322.3873	9.435897	1080.8961
5.154762	393.7222	9.794872	1085.5974
5.285714	461.4555	10.303419	1090.2990
5.416667	524.6311	10.811966	1093.5160
5.547619	582.9870		

$D_e^X = 1102.0714$ cm^{-1}

$R_{out} = 9.49661$ Å $\quad C_8 = 2.4504\times10^8$ cm^{-1} Å^8

$C_6 = 1.074\times10^7$ cm^{-1} Å^6 $\quad C_{10} = 1.1550\times10^{10}$ cm^{-1} Å^{10}

The energy level data set for the B state was complemented by 56 accurate term energies of the levels excited by the Ar^+ and the Nd:YAG lasers in our experiment ($0 \leqslant v' \leqslant 24, 17 \leqslant J' \leqslant 163$). Their uncertainties vary from 0.001 to 0.02 cm^{-1}, but for the fit their statistical weight was set to 0.02 cm^{-1} in order to avoid the influence of possible perturbations (several levels of the B state were found to be perturbed and deviations up to 1.26 cm^{-1} were reported [19]).

In Table V the improved Dunham coefficients for the $B\,^1\Sigma_u^+$ state are listed. They reproduce 367 term energies with a standard deviation of 0.032 cm^{-1} and $\overline{\sigma} = 0.92$. Nine

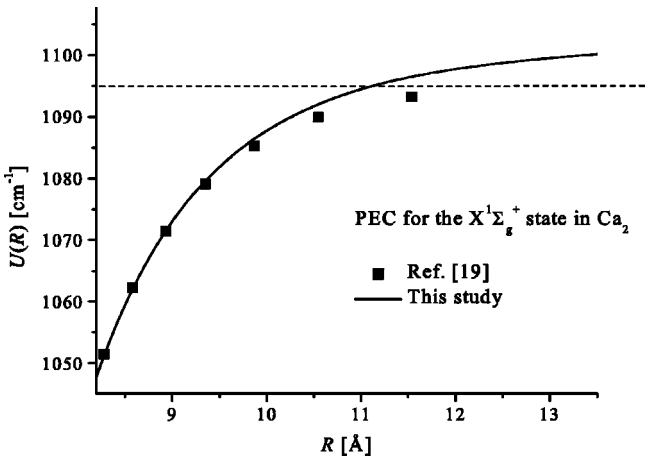

FIG. 7. Comparison between the $^{40}Ca_2$ ground-state potentials from Ref. [19] (squares) and from this study (solid line) near the dissociation limit. The dashed line indicates the old value of the dissociation limit. The outer classical turning point of the last level observed in our experiment is around 13.1 Å.

levels were removed from the fit, because their deviations exceeded twice the experimental uncertainty. Except for possible perturbations, typographic errors or misassignments in the original data lists cannot be excluded, since several such examples were found. T_e is calculated with respect to the minimum of the ground-state potential. In order to avoid possible uncertainty due to the position of the ground-state minimum, we calculated also the value of T_0, i.e., the energy separation between the $(v''=0,J''=0)$ and $(v'=0,J'=0)$ levels, $19\,000.021\pm0.034$ cm^{-1}. It is worth mentioning that the improvement of the B state description at present is limited by the accuracy of the data from Ref. [18], by the single-channel model which excludes the influence of the neighboring states, and also by the presence of collisional level shifts.

TABLE V. Dunham coefficients Y_{00} and T_0 for the $B\,^1\Sigma_u^+$ state in $^{40}Ca_2$ (determined for $0\leqslant v'\leqslant 24, 17\leqslant J'\leqslant 163$, see the text for details). All values are given in cm^{-1}. T_e is calculated with respect to the minimum of the ground-state potential.

T_e+Y_{00}	18964.104(12)
Y_{10}	136.56812(540)
Y_{20}	−0.697074(740)
Y_{30}	$-5.6326(340)\times10^{-3}$
Y_{50}	$-1.0708(200)\times10^{-6}$
Y_{01}	$5.816493(260)\times10^{-2}$
Y_{11}	$-2.95041(590)\times10^{-4}$
Y_{21}	$-3.8762(390)\times10^{-6}$
Y_{41}	$-2.4511(340)\times10^{-9}$
Y_{02}	$-3.989(21)\times10^{-8}$
Y_{12}	$-8.183(120)\times10^{-10}$
Y_{32}	$-1.374(37)\times10^{-12}$
Y_{03}	$-5.124(550)\times10^{-14}$
Y_{00}	−0.045
T_0	19000.021(34)

Further experimental study of the B state is needed to investigate in detail the origins of the observed perturbations, and to extend the description of the state to longer internuclear distances, where already accurate photoassociation data exist [17].

The revised description of the Ca_2 ground state leads to a new value of the B state dissociation energy. Taking the value of T_e from Table V, the separation between the atomic asymptotes (23 652.304 cm^{-1} [32]) and 1102.08 cm^{-1} as a dissociation energy for the X state, for D_e^B one obtains

$$D_e^B = D_e^X + \Delta E(^1P\text{-}^1S) - T_e = 5790.28(9)\ \text{cm}^{-1}. \quad (6)$$

The error is mainly due to the uncertainty of D_e^X. The energy distance between the $(v'=0,J'=0)$ level and the ^1P-^1S asymptote is $D_0^B = 5722.18(9)$ cm^{-1}.

V. CONCLUSIONS

In this paper we report on a spectroscopic study of the ground $X\,^1\Sigma_g^+$ state of $^{40}Ca_2$ by the laser induced fluorescence technique. A total of 730 energy levels were observed $(0\leqslant v''\leqslant 35, 10\leqslant J''\leqslant 164)$, which allowed not only to revise the existing description of the state [19], but also to extend it up to 2.5 cm^{-1} below the dissociation limit. In order to exclude the influence of the possible perturbations of the excited states, only information that concerns the ground state was extracted from the spectra. It was done by comparing the frequencies of the transitions which originate from common excited-state energy levels. Thus one can directly determine the differences between the corresponding ground-state levels.

An accurate potential-energy curve was constructed by using two different representations: analytic and pointwise. They reproduce all the experimental data up to $v''=35$ with a standard deviation $\sigma=0.0065$ cm^{-1}, and $\sigma=0.0068$ cm^{-1}, respectively, which is a significant improvement of the Ca_2 ground-state description, compared to $\sigma=0.036$ cm^{-1} for $v''\leqslant 34$ reported in Ref. [19] (actually we found $\sigma=0.1$ cm^{-1} for $v''\leqslant 29$).

The analysis, based on the constructed PECs and the most recent theoretical value of C_6 [12], sets limits to the value of the dissociation energy of the X state $D_e^X = 1101.99$–1102.17 cm^{-1} [mean value $D_e^X = 1102.08(9)$ cm^{-1}, $D_0^X = 1069.88(9)$ cm^{-1}]. The calculated values of the s-wave scattering length a are between $112a_0$ and $850a_0$ (the Bohr radius $a_0\approx0.52918$ Å). The extreme values of a around $800a_0$ were found for the lowest values of $C_6 = 1.02\times10^7$ cm^{-1} Å^6 and $D_e^X = 1101.99$ cm^{-1}. Small changes of D_e^X to even lower values could lead to negative values of a. It has been already mentioned, however, that lower values of D_e^X are in contradiction with the experimental observations. Therefore we believe that if the deviation of C_6 from the theoretical prediction does not exceed the 5%, limit the stated uncertainty interval for the scattering length is reliable.

For unambiguous determination of the long-range part of the X state PEC, further work is needed. An example of the

experimental technique used for the precise determination of the dissociation energy can be found in Ref. [33]. A possible complementary approach might be to use the photoassociation measurements in Ca_2 [17]. The most recent experiments of the same group [34] covered a significantly wider region of detunings from the ^1S-^1P atomic asymptote (720 MHz–67 GHz, compared to 2.5 GHz–30 GHz in Ref. [17]) and it might be possible to check the parameters of the asymptotic expression for the ground-state potential by comparing the predicted line intensities of the photoassociation spectra with the observed ones (for example, Refs. [35,36]).

The accurate description of the Ca_2 ground-state made it possible to derive also an improved set of Dunham coefficients for the $B\,^1\Sigma_u^+$ state, based on combined data from Ref. [18] and from the present study. The change of D_e^X by more than 7 cm^{-1} as compared to the value determined in Ref. [19], necessitated revision of the dissociation energy of the B state.

ACKNOWLEDGMENTS

This work was supported by DFG through Sonderforschungsbereich SFB 407. The authors are grateful to C. R. Vidal for making available the experimental data from Ref. [18] and to M. Klug for the help during the measurements with the Nd:YAG laser. A.P. kindly acknowledges the research stipend from the Alexander von Humboldt Foundation.

[1] K. Sengstock, U. Sterr, G. Hennig, D. Bettermann, J.H. Muller, and W. Ertmer, Opt. Commun. **103**, 73 (1993).
[2] F. Ruschewitz, J.L. Peng, H. Hinderthur, N. Schaffrath, K. Sengstock, and W. Ertmer, Phys. Rev. Lett. **80**, 3173 (1998).
[3] F. Riehle, H. Schnatz, B. Lipphardt, U. Sterr, T. Binnewies, G. Wilpers, T. Trebst, and J. Helmcke, in *Proceedings of SPIE: Laser Frequency Stabilization, Standards, Measurement, and Applications*, edited by J.L. Hall and J. Ye (SPIE, Bellingham, WA, 2001), Vol. 4269, pp. 112–122.
[4] G. Wilpers *et al.* (private communication).
[5] H. Katori, T. Ido, Y. Isoya, and M. Kuwata-Gonokami, Phys. Rev. Lett. **82**, 1116 (1999).
[6] E.A. Curtis, C.W. Oates, and L. Hollberg, Phys. Rev. A **64**, 031403 (2001).
[7] T. Binnewies, G. Wilpers, U. Sterr, F. Riehle, J. Helmcke, T.E. Mehlstäubler, E.M. Rasel, and W. Ertmer, Phys. Rev. Lett. **87**, 123002 (2001).
[8] T. Ido, Y. Isoya, and H. Katori, Phys. Rev. A **61**, 61403 (2000).
[9] M. Machholm, P.S. Julienne, and K.-A. Suominen, Phys. Rev. A **64**, 033425 (2001).
[10] M. Mérawa, C. Tendero, and M. Rérat, Chem. Phys. Lett. **343**, 397 (2001).
[11] A. Derevianko, Phys. Rev. Lett. **87**, 023002 (2001).
[12] S. Porsev and A. Derevianko, Phys. Rev. A **65**, 020701(R) (2002).
[13] R. Moszynski (private communication).
[14] W.J. Stevens and M. Krauss, J. Chem. Phys. **67**, 1977 (1977).
[15] A.R. Allouche, M. Aubert-Freécon, G. Nicolas, and F. Spiegelmann, Chem. Phys. **200**, 63 (1995).
[16] N. Boutassetta, A.R. Allouche, and M. Aubert-Frécon, Phys. Rev. A **53**, 3845 (1996).
[17] G. Zinner, T. Binnewies, F. Riehle, and E. Tiemann, Phys. Rev. Lett. **85**, 2292 (2000).
[18] W.J. Balfour and R.F. Whitlock, Can. J. Phys. **53**, 472 (1975).
[19] C.R. Vidal, J. Chem. Phys. **72**, 1864 (1980).
[20] C.R. Vidal (private communication).
[21] M.A. Gaveau, M. Briant, P.R. Fournier, J.M. Mestdagh, and J.P. Visticot, J. Chem. Phys. **116**, 955 (2002).
[22] C. Samuelis, E. Tiesinga, T. Laue, M. Elbs, H. Knöckel, and E. Tiemann, Phys. Rev. A **63**, 012710 (2000).
[23] W. Kosman and J. Hinze, J. Mol. Spectrosc. **51**, 341 (1974).
[24] C. Vidal and H. Scheingraber, J. Mol. Spectrosc. **65**, 46 (1977).
[25] A. Pashov, W. Jastrzębski, and P. Kowalczyk, Comput. Phys. Commun. **128**, 622 (2000).
[26] A. Pashov, W. Jastrzębski, and P. Kowalczyk, Comput. Phys. Commun. **113**, 6624 (2000).
[27] W.H. Press, S.A. Teukolski, W.T. Vetterling, and B.P. Flannery, *Numerical Recipes in Fortran 77* (Cambridge Unversity Press, Cambridge, 1992).
[28] A.A. Radzig and P.M. Smirnov, *Reference Data on Atoms, Molecules and Ions* (Springer, Berlin, 1985).
[29] E. Tiesinga, S. Kotochigova, and P.S. Julienne, Phys. Rev. A **65**, 042722 (2002).
[30] P.J. Mohr and B.N. Taylor, Rev. Mod. Phys. **72**, 351 (1998).
[31] G. Audi and A.H. Wapstra, Nucl. Phys. A **A595**, 409 (1995).
[32] S. Bashkin and J.O. Stoner, *Atomic Energy-Level and Grotrian Diagrams* (North-Holland, Amsterdam, 1978, Vol. 2).
[33] M. Elbs, H. Knöckel, T. Laue, C. Samuelis, and E. Tiemann, Phys. Rev. A **59**, 3665 (1999).
[34] C. Degenhardt *et al.* (private communication).
[35] E. Tiesinga, C.J. Williams, P.S. Julienne, K.M. Jones, P.D. Lett, and W.D. Phillips, J. Res. Natl. Inst. Stand. Technol. **101**, 1996 (1996).
[36] H.M.J.M. Boesten, C.C. Tsai, J.R. Gardner, D.J. Heinzen, and B.J. Verhaar, Phys. Rev. A **55**, 636 (1997).